Supplementary Information

High dose-rate brachytherapy of localized prostate cancer converts tumors from cold to hot.

Authors

Simon P Keam[1,2,4*], Heloise Halse[2*], Thu Nguyen[2], Minyu Wang[2], Nicolas Van Kooten Losio[2], Catherine Mitchell[3], Franco Caramia[1], David J Byrne[3], Sue Haupt[1,4], Georgina Ryland[3], Phillip K Darcy[2,4], Shahneen Sandhu[5], Piers Blombery[3,4], Ygal Haupt[1,4,6], Scott G Williams[7#], Paul J Neeson[2,4#].

Supplementary Materials and Methods

1. *Patient cohort and sample collection*
2. *Multiplex IHC*
3. *Multiplex IHC quality control and validation*
4. *Nanostring and 3' RNAseq immune gene expression profiling*
5. *Digital Spatial Profiling*
6. *Data Analysis, bioinformatics and statistical considerations.*

Supplementary Figures

Supplementary Figure S1: Multiplex IHC experimental overview and example of pipeline for quantification of immune subsets in human prostate cancer tissue biopsies. (A) Workflow of experimental multiplex IHC study. (B) H&E stain and corresponding Opal™ tissue classification of non-tumor (blue) and tumor (red). (C) Raw acquired images from either pan-immune (left) or T cell panels (right). Example high magnification (D) non-tumor zone and (E) tumor zone. (F) Deconvoluted and processed images prior to quantification of cell types. (G) Spatial plot of identified immune subtypes indicating assignment of different cell types on the tissue and their spatial relationship.

Supplementary Figure S2: The effect of tumor and non-tumor amount on PCa immune context. Using the segmentation data from Figure S1B, each prostate biopsy was depicted by (A) Total area of pathologically defined tumor and non-tumor (mm^2). (B) Correlation between tumor proportion and total tissue proportion. (C) Correlation between total tissue area and total immune cell density evaluated by multiplex IHC. Corresponding r values are shown with p-values evaluated using Pearsons correlation (95% confidence interval).

Supplementary Figure S3: Pearson's correlation scatterplots of $CD3^+$ cell densities in assessed tissues evaluated using either Pan-immune or T cell panels. Data was divided by either (A) non-tumor or (B) tumor zones. Dots are coloured by either pre- or post-HDRBT state with corresponding Pearson's r values and p-values shown (95% CI).

Supplementary Figure S4: (A) TIS score and (B) immune cell densities according to ADT-treatment status in pre-HDRBT biopsies. Paired t-tests used for statistical analysis with p-values indicated.

Supplementary Figure S5: High dose rate brachytherapy induced a 16-gene tumor inflammatory signature (TIS) in localized PCa. Figure 2A with inclusion of clinical characteristics**.** Shown is (A)

Heatmap of normalized expression levels of 16 genes in tumor inflammatory signature (TIS) and categorisation by k-means clustering into three groups: (i) Cluster 1, high TIS, (ii) Cluster 2, intermediate TIS, and (iii) Cluster 3, Low TIS. Grey and black boxes indicate either pre-HDRBT or post-HDRBT tissue, respectively. Colored circles within grey boxes (pre-HDRBT) indicate post-HDRBT TIS category change. Other clinical parameters are shown above (i.e. Gleason Grade Group, T-stage, relapse status, and ADT pre-treatment).

Supplementary Figure S6: Patient line-matched mean TIS expression levels in pre- or post-HDRBT-treated PCa tissue. Red lines indicate increase, blue lines indicate decrease. Significance assessed using Wilcoxon matched pair test. *p<0.05, ** p<0.01, ***, p<0.001, ****p<0.0001.

Supplementary Figure S7: A pre-existing immune response is associated with a tumor inflammatory signature response to HDRBT. Nanostring immune GEP data was examined on paired pre- and post-HDRBT biopsies. Good responders were classified as those that initially had a low tumor inflammation signature (TIS) pre-HDRBT (15 patients; 65% total patients), but were subsequently converted to an intermediate or high TIS post-HDRBT (n=12/15; 80% of low TIS). Poor responders were classified as those with no post-HDRBT change (n=3/15; 20% of low TIS). (A) Z-score gene expression heatmap of significant changes calculated using a t-test. (B) Bubblechart of gene set enrichment analysis using curated Hallmark datasets and (C) example summary plots from selected immune signalling pathways (bold). (D) mRNA expression levels of IFNγ, IFNα, and TNFβ in samples from two low TIS categories (R: responder and NR: non-responder), and intermediate and high TIS categories.

Supplementary Figure S8: Nanostring immune profiling of post-HDRBT response in prostate tissue from 23 patients. (A) Volcano plot of post-HDRBT changes in 770 changes in Nanostring panel. FDR = false discovery rate. Highly significant candidates (FDR=0) indicated in dotted line box. (B) Magnification of highly (n=57) significant candidates and colour coding according to assigned function according to Nanostring designations or subsequent gene ontology analyses. Gene ontology analysis of candidates (n=59) using (C) Human Gene Atlas or (D) WikiPathways. (E) Volcano plots of discrete immune gene changes sorted by four functional immune classes defined in the nCounter Nanostring Pan Cancer Immune Panel.

Supplementary Figure S9: (B) Box and whisker plots of transcript expression levels of the 8 IHC markers (*CD3E, CD4, CD8A, CD68, ITGAX, MS4A1, FOXP3* and *PDL1*) either pre- or post-HDRBT that were also assessed in multiplex IHC analysis. Differences were assessed using a Wilcoxon matched pair test. *p<0.05, ** p<0.01, ***, p<0.001, ****p<0.0001.

Supplementary Figure S10: Digital spatial profiling supplementary information 1. (A) 4-color (CD3, CD68, DAPI and PanCK) stains of RNA and protein slides with selected ROIS indicated. Scale bar equivalent to 2mm. (B) Flowchart of ROI selection in post-HDRBT tissue in two patients (RB019 and RB023). (C) DSP protein correlation of pan-tumor class (c.f. Figure 4F,G,H)

Supplementary Figure S11: Digital spatial profiling supplementary information 2. IHC of 24 ROIs selected for RNA and protein DSP IO panels. Panels are organised by TIS category determined previously (c.f. Figure 4B).

Supplementary Figure S12: Correlation dot plots of normalized TIS scores and immune cell population densities for all 46 tissues in cohort. Dots are coloured according to Pearson correlation coefficient value.

Supplementary Figure S13: (A) Pearson correlation between immune cell subsets in all biopsies (n=24) using total tissue information (tumor + non-tumor). Squares indicate important associations investigated in B. (B) Representative scatterplot correlations between immune cell subsets. 95% confidence interval from Pearson correlation. (C) Bubblechart of pearson correlations when subcategoriesed by HDRBT status and tissue zone. Only significant (p>0.05) correlations are shown with squares indicating shared correlations between tissue zones.

Supplementary Figure S14: Graphical illustration of median cell distance calculation used for Figure 7.

Materials and Methods

Patient cohort and sample collection

Table 1 shows the clinical characteristics of 24 patients with localized PCa analyzed in this study. Each patient received high-dose-rate brachytherapy (HDRBT) with curative intent, as a boost therapy, prior to external beam radiotherapy (EBRT), using an afterloaded Iridium-192 (^{192}Ir) source (Elekta Flexitron). Brachytherapy was performed using transrectal ultrasound guidance and computed tomography simulation for planning purposes. Patients had two HDRBT treatments performed 14 days apart with a 10Gy fraction prescribed to the target volume (whole prostate) on each occasion, followed by 46Gy in 23 fractions of EBRT. Androgen Deprivation Therapy (ADT) using a Luteinising Hormone Releasing Hormone agonist was administered for 4 months prior to the radiotherapy in six of these cases. All participants provided consent covering tissue research as part of a prospective tissue collection study for prostate radiobiology research, approved by the Human Research Ethics Committee at the Peter MacCallum Cancer Centre (PMCC; HREC approvals 10/68, 13/167, 18/204).

Ultrasound-guided prostate biopsies were obtained using a 16G biopsy system (Bard Magnum series) immediately before the first fraction of HDRBT and 14 days later, prior to the second fraction and consequently represent the 2-week response of the PCa to a single 10Gy HDRBT fraction. Prostate biopsies were conducted using a template-based transperineal approach that enabled repeated sampling with millimeter precision. Areas of interest for sampling were selected using all available factors including: knowledge of cancer location based on prior biopsy location positivity; imaging results such as MRI or PET scanning (where available); the location of a nodule on examination; and any region of abnormality detected by ultrasound at the time of biopsy. Integration of these clinical and imaging factors was performed at the time of biopsy by the procedural clinician. Multiple biopsies (typically 3-5) were taken through the likely tumor-bearing regions of the prostate with the subsequent repeat samples taken from the same spatial coordinates within the gland. Tissue cores were fixed immediately by immersion in a solution of 10% neutral buffered formaldehyde for a maximum of 24 hours at room temperature, prior to paraffin-embedding. Representative 3μm sections were acquired from all paraffin blocks for routine staining for light microscopy and high-resolution scanning. All cores were examined by a uro-pathologist for tumor location and histopathology features described, in addition to an updated ISUP Gleason grade group scoring system, T-stage, and androgen treatment status.

Multiplex IHC

Our study was achieved using two staining and computational analysis platforms following technical advancements in the multiplex IHC pipeline during the course of the study. Repeat analysis of already assessed tissues using the updated procedures was not permissible due to the exhaustion of the strictly limited tissue resources.

All prostate core biopsies were formalin fixed and paraffin embedded (FFPE). Subsequently, serial 3 µm sections were cut with H&E stained slides from each FFPE block evaluated by a uropathologist who defined 'tumor' vs 'non-tumor' prostate tissue regions. This region of interest was based on the presence of ≥2 definitive tumor glands in the area. Single tumor cells and glands were not considered tumor areas. The adjacent 3 µm FFPE tissue section from each biopsy was mounted on a Trajan Series 3 adhesive slide, deparaffinized and rehydrated by serial passage through changes of xylene and graded ethanol for multiplex immunohistochemistry staining with the T cell Panel and Pan Immune Panel as described previously [1]**.** In brief, the T cell Panel included: DAPI, CD3, CD4, CD8, FOXP3 and PDL1. The Pan-immune Panel consisted of DAPI, HMWCK, CD3 (T cells), CD20 (B cells), CD11c (dendritic cells; DC), CD68 (macrophages; Mφ) and PDL1 with inferred phenotypes outlined in **Table 2**. An overview of the multiplex IHC pipeline is provided in **Supplementary Figure S1A**.

Manual and automated staining was performed on Cohorts A and B, respectively. The manual protocol starts with primary heat-induced epitope retrieval (HIER), where tissue sections were incubated in 1 mM EDTA buffer, pH 8.0 125°C for 3 minutes Subsequent HIERs were dependent on antibody used and performed in the microwave at 90°C, 10% power for 15 minutes. Antibodies used included rabbit monoclonal CD4 (Spring Bioscience, clone SP35, 1/100, high pH retrieval), rabbit monoclonal CD3 (Spring Bioscience, clone SP7, 1/1000, low pH retrieval), mouse monoclonal CD8 (Thermofisher, clone 4B11, 1/1000, high pH retrieval), rabbit polyclonal FOXP3 (BioSB, 1/100, high pH retrieval), rabbit monoclonal PDL1 (Spring Bioscience, clone SP142, 1/1000, high pH retrieval), mouse monoclonal

HMWCK (DAKO, clone 34βE12, 1/500 titre and low pH retrieval), mouse monoclonal CD20 (DAKO, clone L26, 1/500, low pH retrieval), mouse monoclonal CD68 (Thermofisher, clone 514H12, 1/200, high pH retrieval), and rabbit monoclonal CD11c (BioSB, clone EP157, 1/2000, low pH retrieval). Endogenous peroxidase in tissues was blocked by incubation of slides in 3% hydrogen peroxide solution after incubation with primary antibody. Immunofluorescent signal was visualized using the OPAL™ 7-color fIHC kit (Perkin Elmer, MA) TSA dyes 520, 540, 570, 620, 650, and 690, counterstained with Spectral DAPI. All steps in the manual protocol were optimized for the Leica BOND RX autostainer for Cohort B.

All slides were subsequently imaged on the Vectra® 3.0 Automated Quantitative Pathology Imaging System, 200 slide (Perkin Elmer, MA). Slides were scanned at 10X magnification in order to select for high-powered imaging at 20X (resolution of 0.5 µm per pixel) using Phenochart (Perkin Elmer MA). Tissue classification for cohort A was informed directly by histopathological definitions of tumor-enriched and non-tumorl-enriched tissue zones by a trained uropathologist. Entire prostate cores from Cohort B were imaged on the Vectra® due to advancements made with the HALO® Image Analysis Platform v2.3 (Indica Labs) that allowed for whole tissue analysis.

Alterations between the two analysis methods included the primary use of inForm® Software v2.2 for Cohort A and the combination of inForm® Software v2.4 and HALO® for Cohort B. The analysis pipeline on inForm® v2.2 (Perkin Elmer, MA) started with the deconvolution of fluors, tissue and cell segmentation and cell phenotyping. This method later evolved for Cohort B, where the deconvoluted files from Inform 2.4 were exported into HALO® and merged to produce the whole core biopsy. Tissue and cell segmentation and cell phenotyping were performed using the Highplex v2 module on the HALO® software,

Cell segmentation in both softwares was done based on all cells counter-stained with DAPI. Manual annotations in HALO® segmented the tissue into tumour- and non-tumorl-enriched areas guided by uropathologist markups of the H&E stained biopsies. Cell phenotyping on inForm® was undertaken by selecting at least 5 representative cells per phenotype, then performing reiterations until at least 20 representative cells per phenotype were selected. Batch analysis was performed on all high-powered images of prostate tissue using the same algorithm designed on one representative image per metastasis, to account for staining variability and intensity between patients. Cell phenotyping on HALO® was performed by thresholding the individual seven markers in the panel for each slide. A real-time tuning window allowed the threshold settings to be adjusted and this window was moved to all regions around the core before the entire tissue was analyzed. Density of cell subsets was subsequently calculated per mm^2 in all fields per tissue class (Cohort A) or whole tissue acquisition (Cohort B). An example of the experimental pipeline is shown for Cohort B in **Supplementary Figure S1B-G**.

Multiplex IHC quality control and validation

As PCa is a highly heterogeneous and infiltrative disease, we examined the relative amount of tumor in each biopsy in the larger cohort B of 17 patients. This analysis, shown in **Supplementary Figure S2A**, revealed a large distribution in total biopsy size (2.8 – 47.3 mm^2: mean of 21.4 mm^2) and relative proportion of tumor (0.7% – 100%; mean of 25.8%). Importantly, the analysis showed no relationship between biopsy size and tumor content (**Supplementary Figure S2B**), or total area and subsequent total immune cell densities (**Supplementary Figure S2C**). Seven biopsies did not contain any defined tumor zones, which is a common observation in prostate cancer. For the purposes of this analysis, these tissues are still considered to be adjacent to tumor cells and therefore 'non-tumor' due to other adjacent sections demonstrating the presence of tumor. As demonstrated in **Figure 1B**, we use tumor/non-tumor tissue designation and *in silico* classification to explore the role of tumor zones in driving differential tumor responses in downstream mIHC analyses. An advantage of our analysis was the ability to evaluate the expression of common markers on both panels. Specifically, this included the relative number of CD3+ cells (pan-immune panel) and the summation of CD3+ T cell subsets (T cell panel). The results, shown in **Supplementary Figure S3**, showed significant concordance between the two mIHC panels regardless of radiation or tumor-bearing status; highlighting the robust nature of the pipeline. Androgen deprivation pre-treatment (ADT) was used as concurrent treatment for 6 patients in the cohort. We identified that no statistically significant (student's t-test) differences at baseline between ADT-treated and untreated tissues for both TIS expression and immune cell subset densities (**Supplementary Figure S4A and B**, respectively).

Nanostring and 3' RNAseq immune gene expression profiling

RNA was isolated and purified from 10 µm tissue sections using the RNeasy FFPE kit (Qiagen) according to the manufacturer's instructions. RNA was eluted from columns in 20µl DEPC treated water. 1µl of RNA from validation samples were tested for quality using a High Sensitivity RNA TapeStation assay (Agilent) with a DV_{200} cutoff of > 50% for downstream analysis. 150 ng total RNA from each patient biopsy was analyzed using the Nanostring platform and the nCounter PanCancer Immune Profiling Panel (Nanostring; NS_CANCERIMMUNE_V1.1 and NS_CANCERIMMUNE_C2929) with downstream normalization and gene quantification performed using nSolver Analysis Software v4.0. Nanostring data from one patient pair was not obtained due to sample exhaustion. Using RNA generated previously, we performed whole transcriptome profiling as per our previous studies [2, 3]. Gene levels were derived from sequenced libraries following batch normalization using limma R package.

Digital Spatial Profiling

3 µm serial sections of post-HDRBT biopsies from patients RB019 and RB023 were processed by Nanostring Technologies using the ImmunoOncology (IO) RNA and protein panels and analyzed using a GeoMx. Sections were stained prior to ROI selection (12 ROIs per section) with CD3, CD68, Pan-Cytokeratin (PanCK) and DAPI to enable rational selection of regions. Raw data was normalized to both External RNA Control Consortium (ERCC) spike-in and signal-to-noise control. These normalized data were used for generation of TIS signature (mean of all normalized values in TIS signature).

Data Analysis, bioinformatics and statistical considerations.

Data visualization, principle component analysis and t-test volcano plots were performed using Perseus computational platform (version 1.5.6) from the Max Planck Institute of Biochemistry [4]. Heatmaps were generated using mean z-score normalized $\log_2$ Nanostring expression matrices. Volcano plot analysis was performed using a two-sided t-test with 250 randomizations, a false discovery rate (FDR) of 0.05 and an S0 of 0.1. Candidate lists were comprised of genes with p-values < 0.05 and/or an FDR < 0.05. Gene enrichment was performed using the Enricher analysis database using candidates generated previously. We acknowledge our use of the gene set enrichment analysis, GSEA software, and Molecular Signature Database (MSigDB) according to established protocols [5].

R packages implemented included *corrPlot* Pearson correlations calculations and visualizations, expression and density visualization were generated using *ggplot2*. Statistical tests utilized included non-parametric Wilcoxon signed-rank test for matched samples, Chi-squared tests for categories, and Pearson r correlations using 99% CI thresholds for correlation studies. P-values are indicated were appropriate. Unless otherwise stated, p-value thresholds were *p<0.05, ** p<0.01, *** p<0.001 and **** p<0.0001. Multivariate analysis was performed in R using stats package aov function.

The 16-gene TIS gene signature was generated from the full 18-gene TIS signature as previously published [6] using data collected using the Nanostring PanCancer Immune Profiling panel. Two genes were not present on the pane l– HLA-DRB1 and NKG7, and are therefore absent. TIS values were generated using mean $\log_2$-transformed normalized expression values for each of the 16 genes assessed, and z-score transformed where appropriate.

The Inter-cellular Spatial Analysis Tool (ISAT) package (version 1.0.5) was used for the distance analysis using R software (version 3.6.1 for Windows). The *x* and *y* coordinates from the HALO (v2.3) raw data were used to calculate the median distance (µm) between two cell nuclei for all tissue types and segmented by tissue zone. Each cell of the same phenotype was used as a reference cell to calculate its distance to the nearest cell of the same cell phenotype as well as different phenotypes in the same mIHC panel.

Power calculations were performed using characteristics of pilot data for Nanostring (used for TIS and candidate identification) and immune subset densities to guide our experimental strategy. The high heterogeneity in immune subset densities between patients resulted in large cohort sizes (n=100-450) needed to achieve high power (0.8). This meant that although could identify radiosensitive immune subsets, we could conclusively determine if immune subsets were radiation insensitive. Conversely, the Nanostring analysis was well-powered due to lower heterogeneity (alpha = 0.05, power = 0.87). We therefore arranged our study to use gene expression profiling (Nanostring-TIS) to initiate our study and complement these data with multiplex IHC.

Figure S1

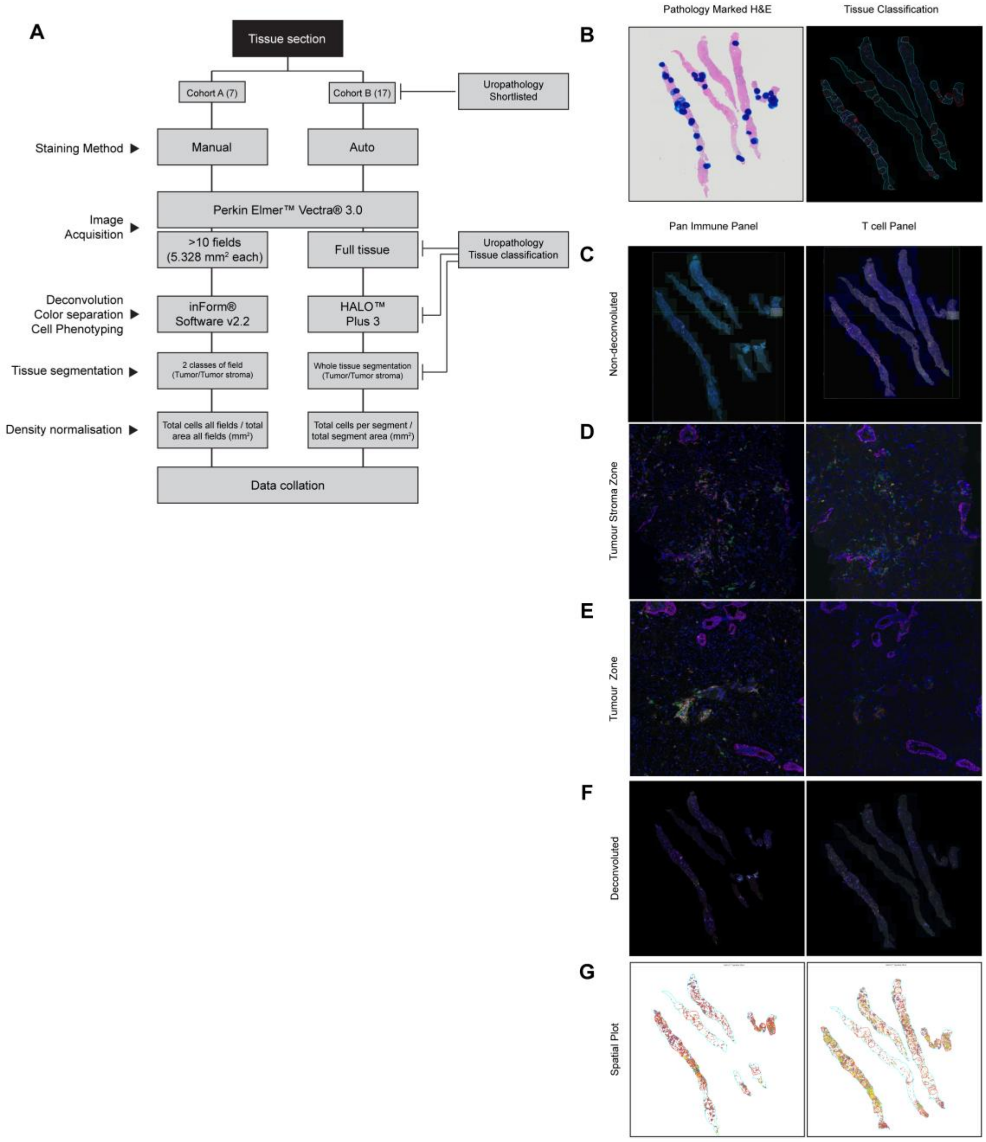
A
Tissue section
Cohort A (7)
Cohort B (17)
Uropathology Shortlisted
Staining Method
Manual
Auto
Image Acquisition
Perkin Elmer™ Vectra® 3.0
>10 fields (5.328 mm² each)
Full tissue
Uropathology Tissue classification
Deconvolution Color separation Cell Phenotyping
inForm® Software v2.2
HALO™ Plus 3
Tissue segmentation
2 classes of field (Tumor/Tumor stroma)
Whole tissue segmentation (Tumor/Tumor stroma)
Density normalisation
Total cells all fields / total area all fields (mm²)
Total cells per segment / total segment area (mm²)
Data collation
B
Pathology Marked H&E
Tissue Classification
C
Pan Immune Panel
T cell Panel
Non-deconvoluted
D
Tumour Stroma Zone
E
Tumour Zone
F
Deconvoluted
G
Spatial Plot

Figure S2

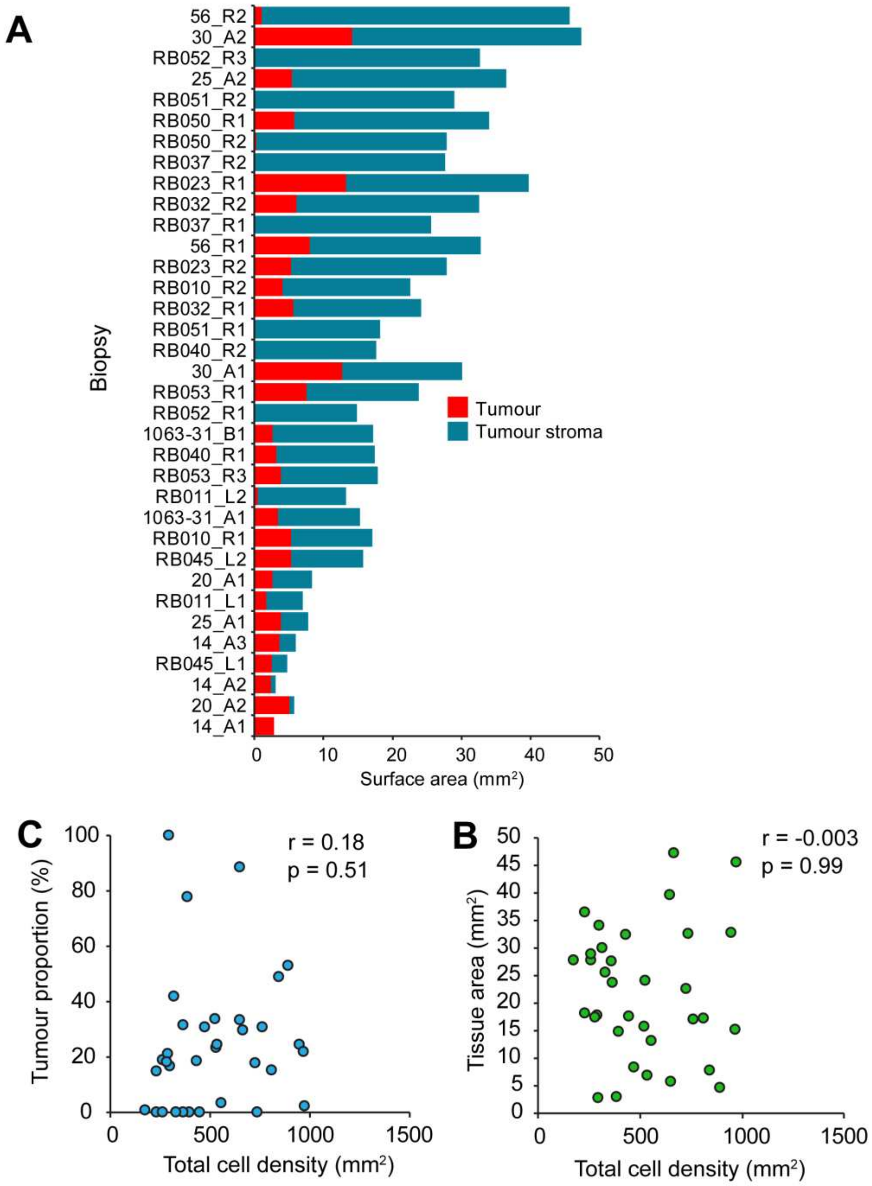
A
56_R2
30_A2
RB052_R3
25_A2
RB051_R2
RB050_R1
RB050_R2
RB037_R2
RB023_R1
RB032_R2
RB037_R1
56_R1
RB023_R2
RB010_R2
RB032_R1
RB051_R1
RB040_R2
30_A1
RB053_R1
RB052_R1
1063-31_B1
RB040_R1
RB053_R3
RB011_L2
1063-31_A1
RB010_R1
RB045_L2
20_A1
RB011_L1
25_A1
14_A3
RB045_L1
14_A2
20_A2
14_A1
Biopsy
Tumour
Tumour stroma
0
10
20
30
40
50
Surface area (mm²)
C
r = 0.18
p = 0.51
Tumour proportion (%)
100
80
60
40
20
0
0
500
1000
1500
Total cell density (mm²)
B
r = -0.003
p = 0.99
Tissue area (mm²)
50
45
40
35
30
25
20
15
10
5
0
0
500
1000
1500
Total cell density (mm²)

Figure S3

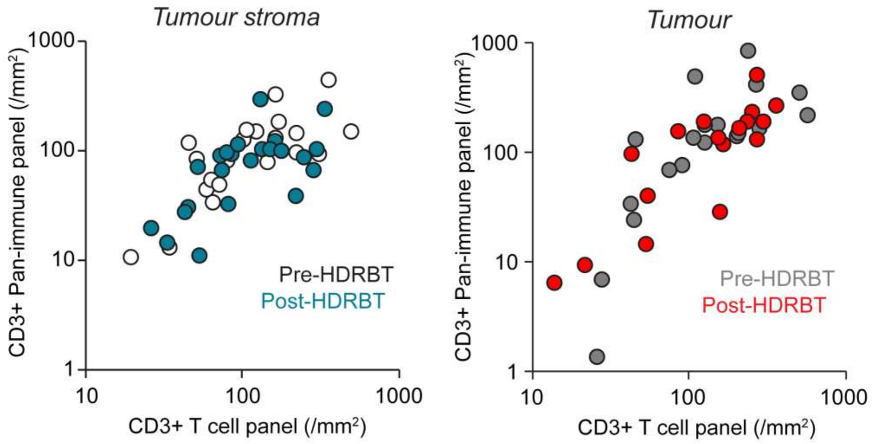

Pearson (95% CI)

Pre-HDRBT (r=0.598, *p*=0.002)
Post-HDRBT (r=0.491, p=0.015)

Pre-HDRBT (r=0.526, *p*=0.008)
Post-HDRBT (r=0.706, *p<0.0002*)

Figure S4

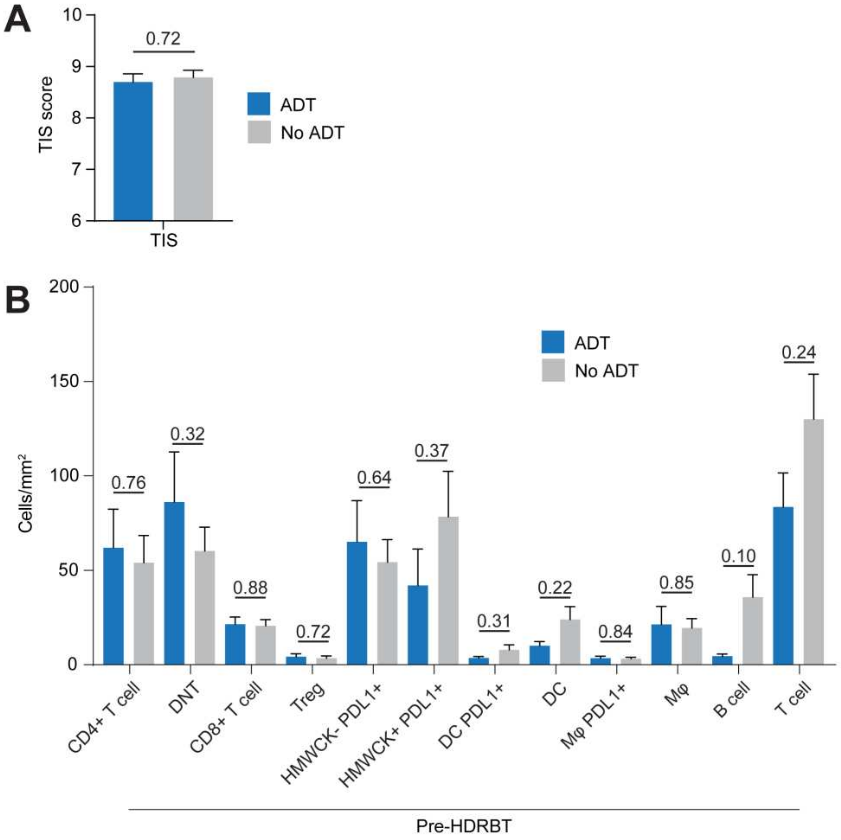
A
10
9
8
7
6
TIS score
0.72
TIS
ADT
No ADT
B
200
150
100
50
0
Cells/mm^2
ADT
No ADT
0.76
0.32
0.88
0.72
0.64
0.37
0.31
0.22
0.84
0.85
0.10
0.24
CD4+ T cell
DNT
CD8+ T cell
Treg
HMWCK- PDL1+
HMWCK+ PDL1+
DC PDL1+
DC
Mφ PDL1+
Mφ
B cell
T cell
Pre-HDRBT

Figure S5

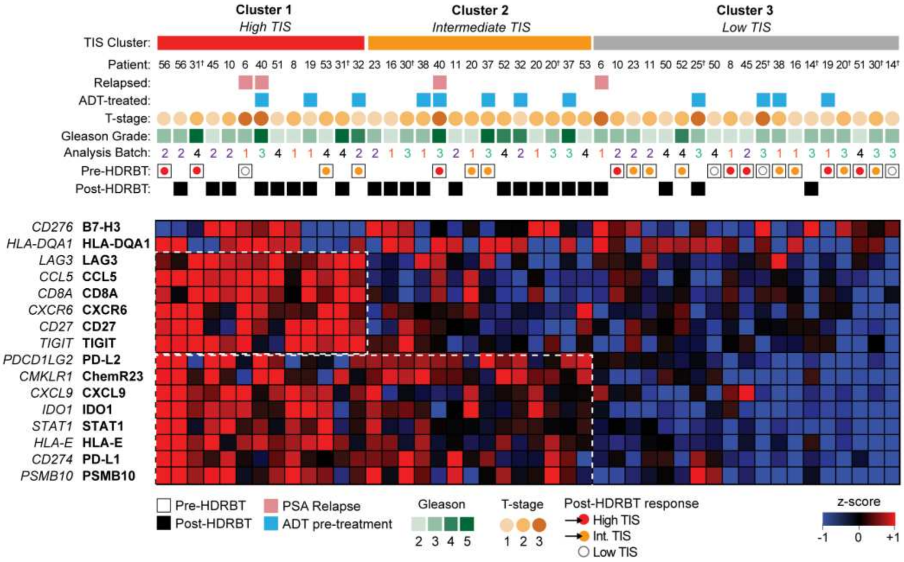
Cluster 1
High TIS
Cluster 2
Intermediate TIS
Cluster 3
Low TIS
TIS Cluster:
Patient: 56 56 31† 45 10 6 40 51 8 19 53 31† 32 23 16 30† 38 40 11 20 37 52 32 20 20† 37 53 6 10 23 11 50 52 25† 50 8 45 25† 38 16 14† 19 20† 51 30† 14†
Relapsed:
ADT-treated:
T-stage:
Gleason Grade:
Analysis Batch: 2 2 4 2 2 1 3 4 1 1 4 4 2 2 1 3 1 3 2 1 3 4 2 1 3 3 4 1 2 2 2 4 4 3 4 1 2 3 1 1 3 1 3 4 3 3
Pre-HDRBT:
Post-HDRBT:
CD276 B7-H3
HLA-DQA1 HLA-DQA1
LAG3 LAG3
CCL5 CCL5
CD8A CD8A
CXCR6 CXCR6
CD27 CD27
TIGIT TIGIT
PDCD1LG2 PD-L2
CMKLR1 ChemR23
CXCL9 CXCL9
IDO1 IDO1
STAT1 STAT1
HLA-E HLA-E
CD274 PD-L1
PSMB10 PSMB10
Pre-HDRBT
Post-HDRBT
PSA Relapse
ADT pre-treatment
Gleason
2 3 4 5
T-stage
1 2 3
Post-HDRBT response
High TIS
Int. TIS
Low TIS
z-score
-1 0 +1

Figure S6

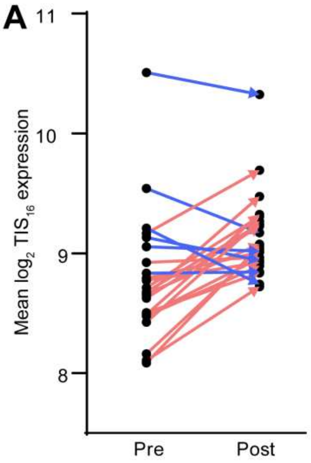

Figure S7

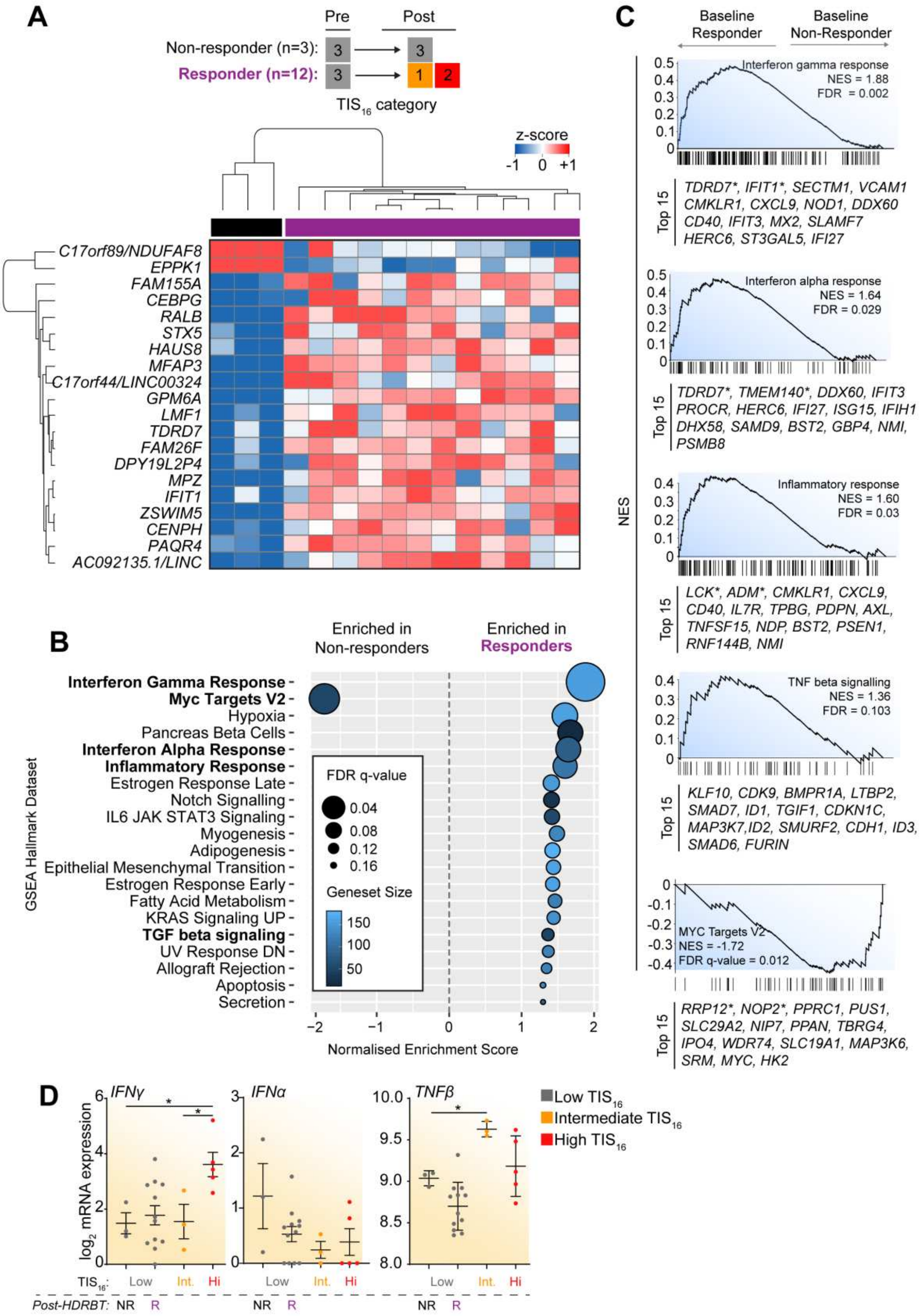
A
Pre
Post
Non-responder (n=3):
3
3
Responder (n=12):
3
1
2
TIS16 category
z-score
-1 0 +1
C17orf89/NDUFAF8
EPPK1
FAM155A
CEBPG
RALB
STX5
HAUS8
MFAP3
C17orf44/LINC00324
GPM6A
LMF1
TDRD7
FAM26F
DPY19L2P4
MPZ
IFIT1
ZSWIM5
CENPH
PAQR4
AC092135.1/LINC
B
Enriched in Non-responders
Enriched in Responders
GSEA Hallmark Dataset
Interferon Gamma Response
Myc Targets V2
Hypoxia
Pancreas Beta Cells
Interferon Alpha Response
Inflammatory Response
Estrogen Response Late
Notch Signalling
IL6 JAK STAT3 Signaling
Myogenesis
Adipogenesis
Epithelial Mesenchymal Transition
Estrogen Response Early
Fatty Acid Metabolism
KRAS Signaling UP
TGF beta signaling
UV Response DN
Allograft Rejection
Apoptosis
Secretion
FDR q-value
0.04
0.08
0.12
0.16
Geneset Size
150
100
50
-2 -1 0 1 2
Normalised Enrichment Score
C
Baseline Responder
Baseline Non-Responder
NES
Interferon gamma response
NES = 1.88
FDR = 0.002
Top 15
TDRD7*, IFIT1*, SECTM1, VCAM1 CMKLR1, CXCL9, NOD1, DDX60 CD40, IFIT3, MX2, SLAMF7 HERC6, ST3GAL5, IFI27
Interferon alpha response
NES = 1.64
FDR = 0.029
Top 15
TDRD7*, TMEM140*, DDX60, IFIT3 PROCR, HERC6, IFI27, ISG15, IFIH1 DHX58, SAMD9, BST2, GBP4, NMI, PSMB8
Inflammatory response
NES = 1.60
FDR = 0.03
Top 15
LCK*, ADM*, CMKLR1, CXCL9, CD40, IL7R, TPBG, PDPN, AXL, TNFSF15, NDP, BST2, PSEN1, RNF144B, NMI
TNF beta signalling
NES = 1.36
FDR = 0.103
Top 15
KLF10, CDK9, BMPR1A, LTBP2, SMAD7, ID1, TGIF1, CDKN1C, MAP3K7,ID2, SMURF2, CDH1, ID3, SMAD6, FURIN
MYC Targets V2
NES = -1.72
FDR q-value = 0.012
Top 15
RRP12*, NOP2*, PPRC1, PUS1, SLC29A2, NIP7, PPAN, TBRG4, IPO4, WDR74, SLC19A1, MAP3K6, SRM, MYC, HK2
D
log2 mRNA expression
IFNγ
IFNα
TNFβ
*
*
*
TIS16:
Low
Int.
Hi
Post-HDRBT:
NR
R
Low TIS16
Intermediate TIS16
High TIS16

Figure S8

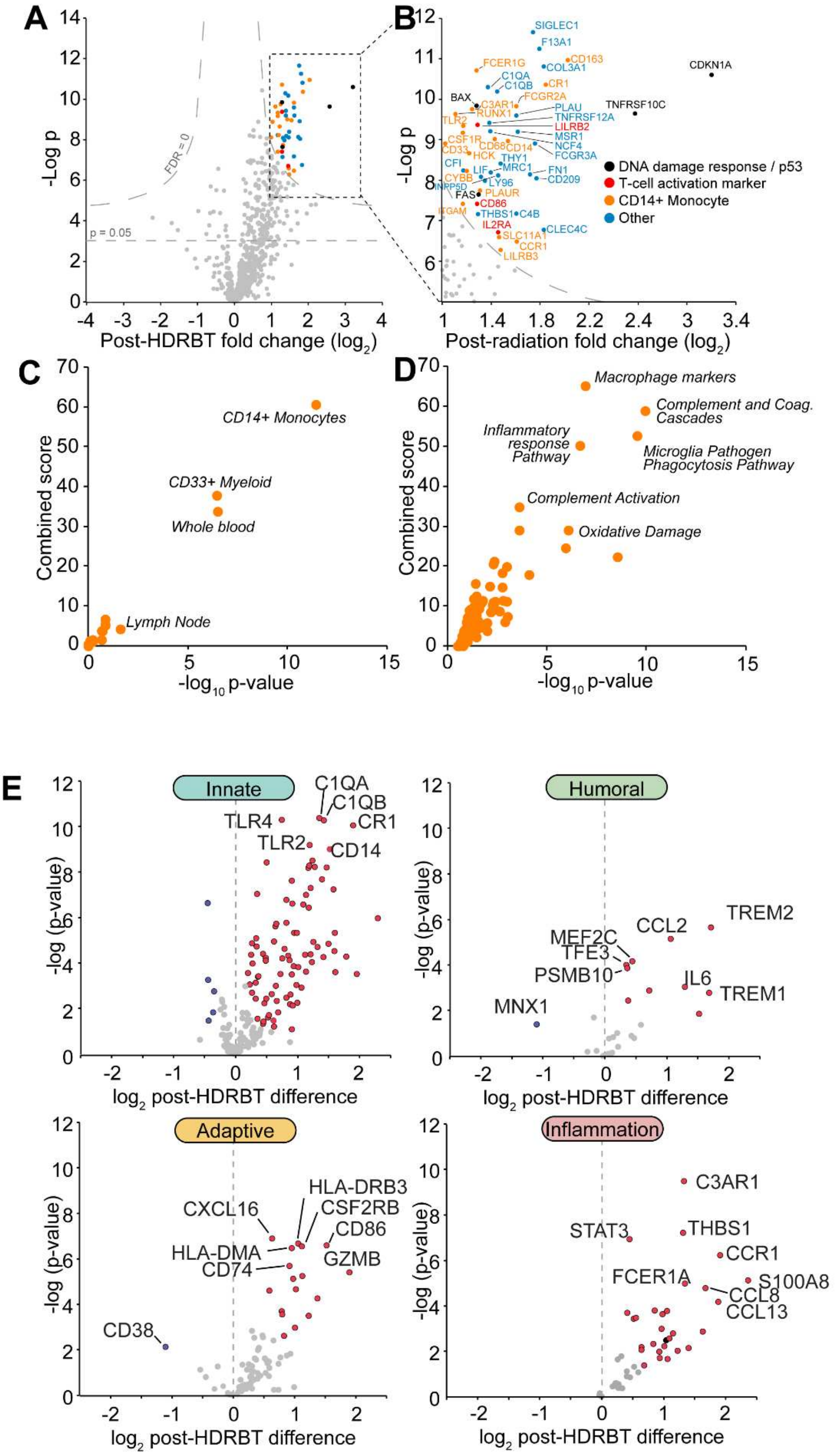
A
14
12
10
8
6
4
2
0
-Log p
FDR = 0
p = 0.05
-4 -3 -2 -1 0 1 2 3 4
Post-HDRBT fold change (log2)
B
12
11
10
9
8
7
6
-Log p
SIGLEC1
F13A1
CD163
FCER1G
COL3A1
CDKN1A
C1QA
C1QB
CR1
FCGR2A
BAX
C3AR1
PLAU
TNFRSF10C
RUNX1
TNFRSF12A
TLR2
LILRB2
MSR1
CSF1R
NCF4
CD68
CD14
CD33
HCK
FCGR3A
THY1
CFI
MRC1
LIF
FN1
CYBB
LY96
CD209
INPP5D
FAS
PLAUR
CD86
THBS1
C4B
ITGAM
IL2RA
CLEC4C
SLC11A1
CCR1
LILRB3
● DNA damage response / p53
● T-cell activation marker
● CD14+ Monocyte
● Other
1 1.4 1.8 2.2 2.4 3 3.4
Post-radiation fold change (log2)
C
70
60
50
40
30
20
10
0
Combined score
CD14+ Monocytes
CD33+ Myeloid
Whole blood
Lymph Node
0 5 10 15
-log10 p-value
D
70
60
50
40
30
20
10
0
Combined score
Macrophage markers
Complement and Coag. Cascades
Inflammatory response Pathway
Microglia Pathogen Phagocytosis Pathway
Complement Activation
Oxidative Damage
0 5 10 15
-log10 p-value
E
Innate
12
10
8
6
4
2
0
-log (p-value)
C1QA
C1QB
TLR4
CR1
TLR2
CD14
-2 -1 0 1 2
log2 post-HDRBT difference
Humoral
12
10
8
6
4
2
0
-log (p-value)
TREM2
CCL2
MEF2C
TFE3
PSMB10
IL6
TREM1
MNX1
-2 -1 0 1 2
log2 post-HDRBT difference
Adaptive
12
10
8
6
4
2
0
-log (p-value)
HLA-DRB3
CXCL16
CSF2RB
CD86
HLA-DMA
GZMB
CD74
CD38
-2 -1 0 1 2
log2 post-HDRBT difference
Inflammation
12
10
8
6
4
2
0
-log (p-value)
C3AR1
STAT3
THBS1
CCR1
FCER1A
S100A8
CCL8
CCL13
-2 -1 0 1 2
log2 post-HDRBT difference

Figure S9

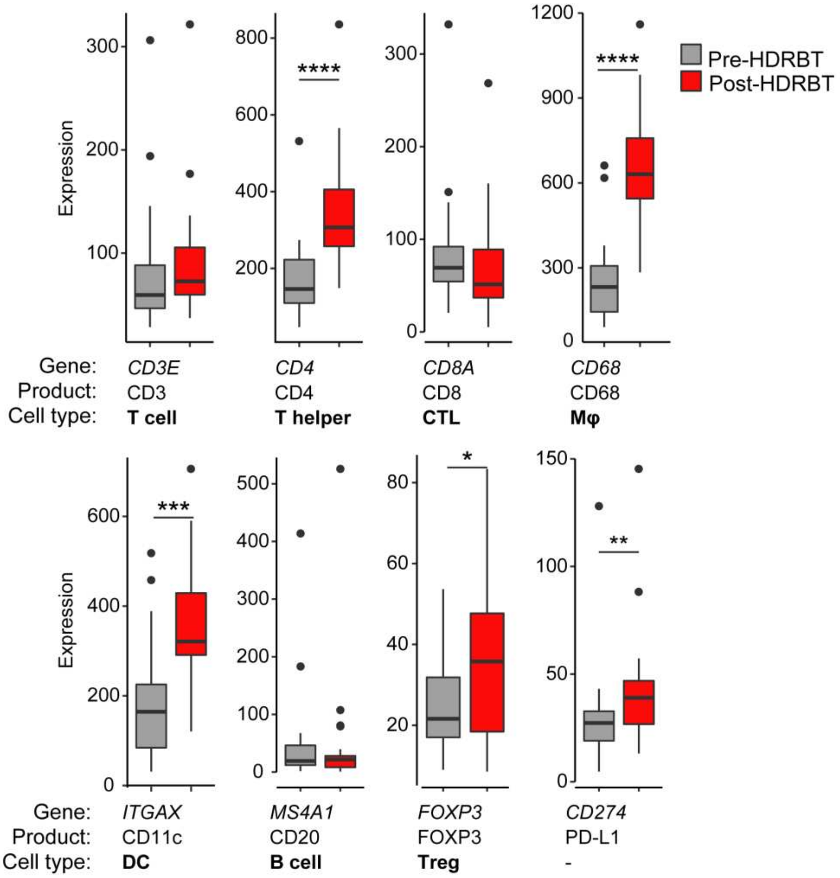
Pre-HDRBT
Post-HDRBT
Expression
300
200
100
800
600
400
200
****
300
200
100
0
1200
900
600
300
0
****
Gene:
Product:
Cell type:
CD3E
CD3
T cell
CD4
CD4
T helper
CD8A
CD8
CTL
CD68
CD68
Mφ
Expression
600
400
200
0
***
500
400
300
200
100
0
80
60
40
20
*
150
100
50
0
**
Gene:
Product:
Cell type:
ITGAX
CD11c
DC
MS4A1
CD20
B cell
FOXP3
FOXP3
Treg
CD274
PD-L1
-

Figure S10

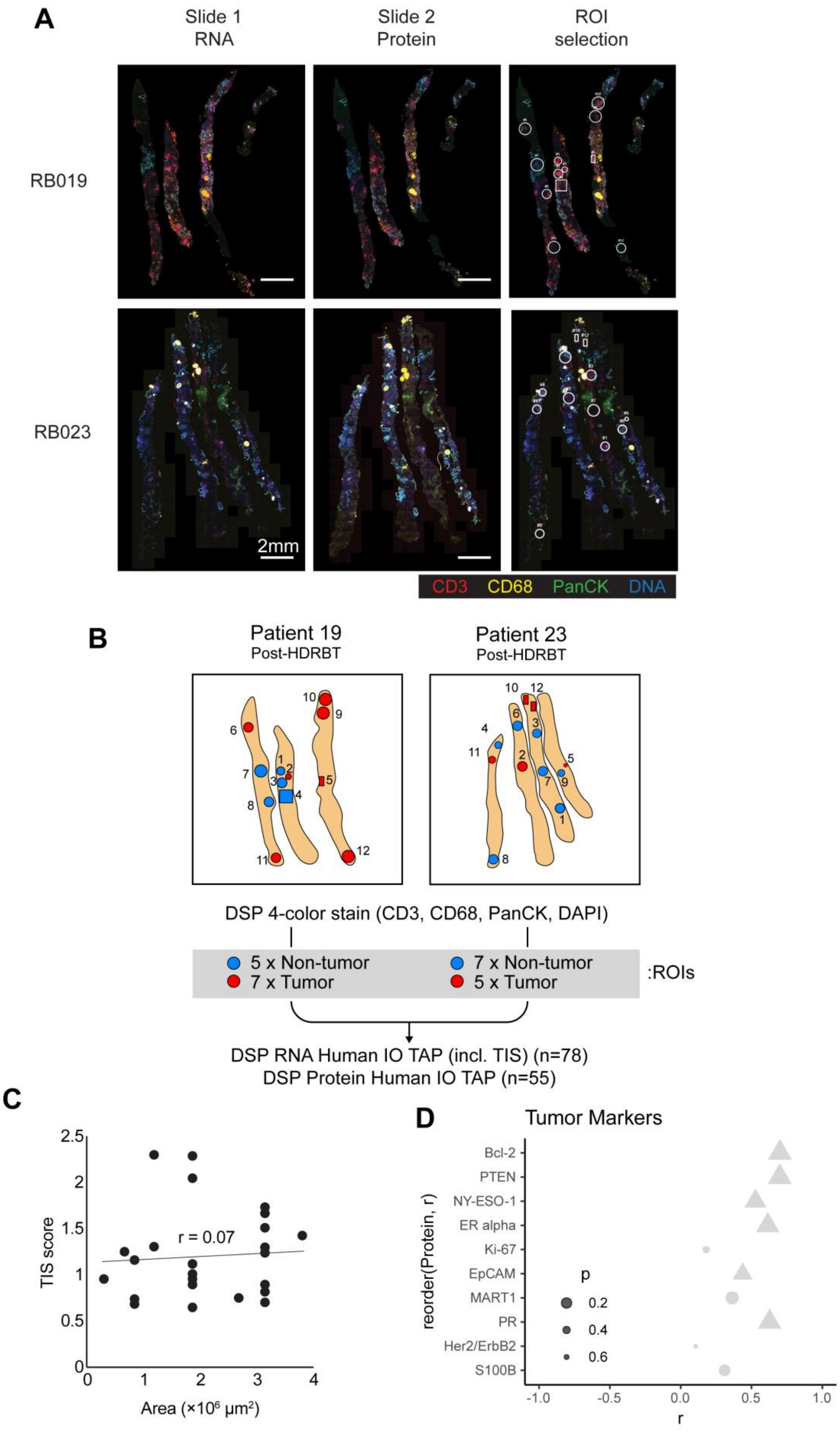
A
Slide 1
RNA
Slide 2
Protein
ROI
selection
RB019
RB023
2mm
CD3
CD68
PanCK
DNA
B
Patient 19
Post-HDRBT
Patient 23
Post-HDRBT
1
2
3
4
5
6
7
8
9
10
11
12
DSP 4-color stain (CD3, CD68, PanCK, DAPI)
5 x Non-tumor
7 x Tumor
7 x Non-tumor
5 x Tumor
:ROIs
DSP RNA Human IO TAP (incl. TIS) (n=78)
DSP Protein Human IO TAP (n=55)
C
TIS score
2.5
2
1.5
1
0.5
0
r = 0.07
0
1
2
3
4
Area (×10⁶ μm²)
D
Tumor Markers
reorder(Protein, r)
Bcl-2
PTEN
NY-ESO-1
ER alpha
Ki-67
EpCAM
MART1
PR
Her2/ErbB2
S100B
p
0.2
0.4
0.6
-1.0
-0.5
0.0
0.5
1.0
r

Figure S11

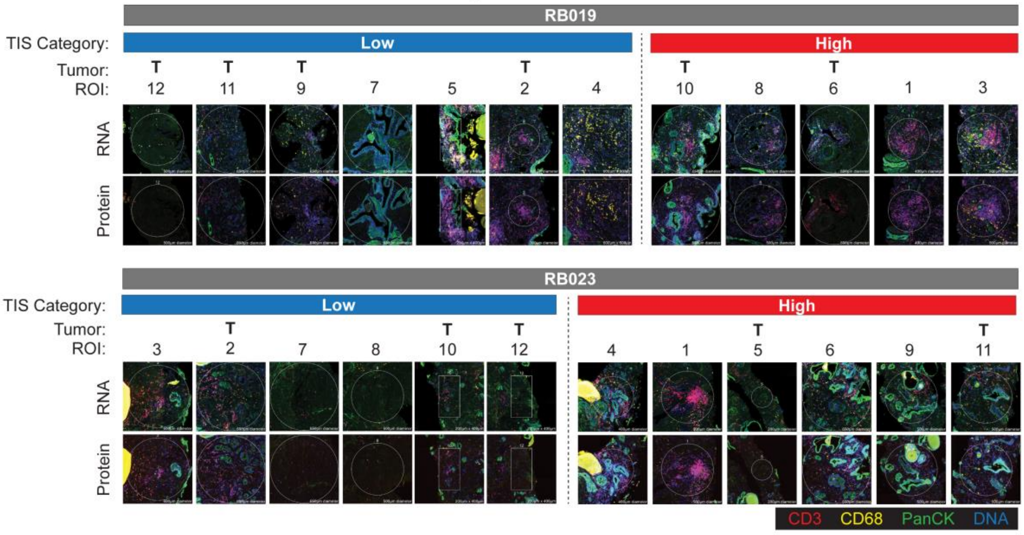
RB019
TIS Category:
Low
High
Tumor:
ROI:
T 12
T 11
T 9
7
5
T 2
4
T 10
8
T 6
1
3
RNA
Protein
RB023
TIS Category:
Low
High
Tumor:
ROI:
3
T 2
7
8
T 10
T 12
4
1
T 5
6
9
T 11
RNA
Protein
CD3 CD68 PanCK DNA

Figure S12

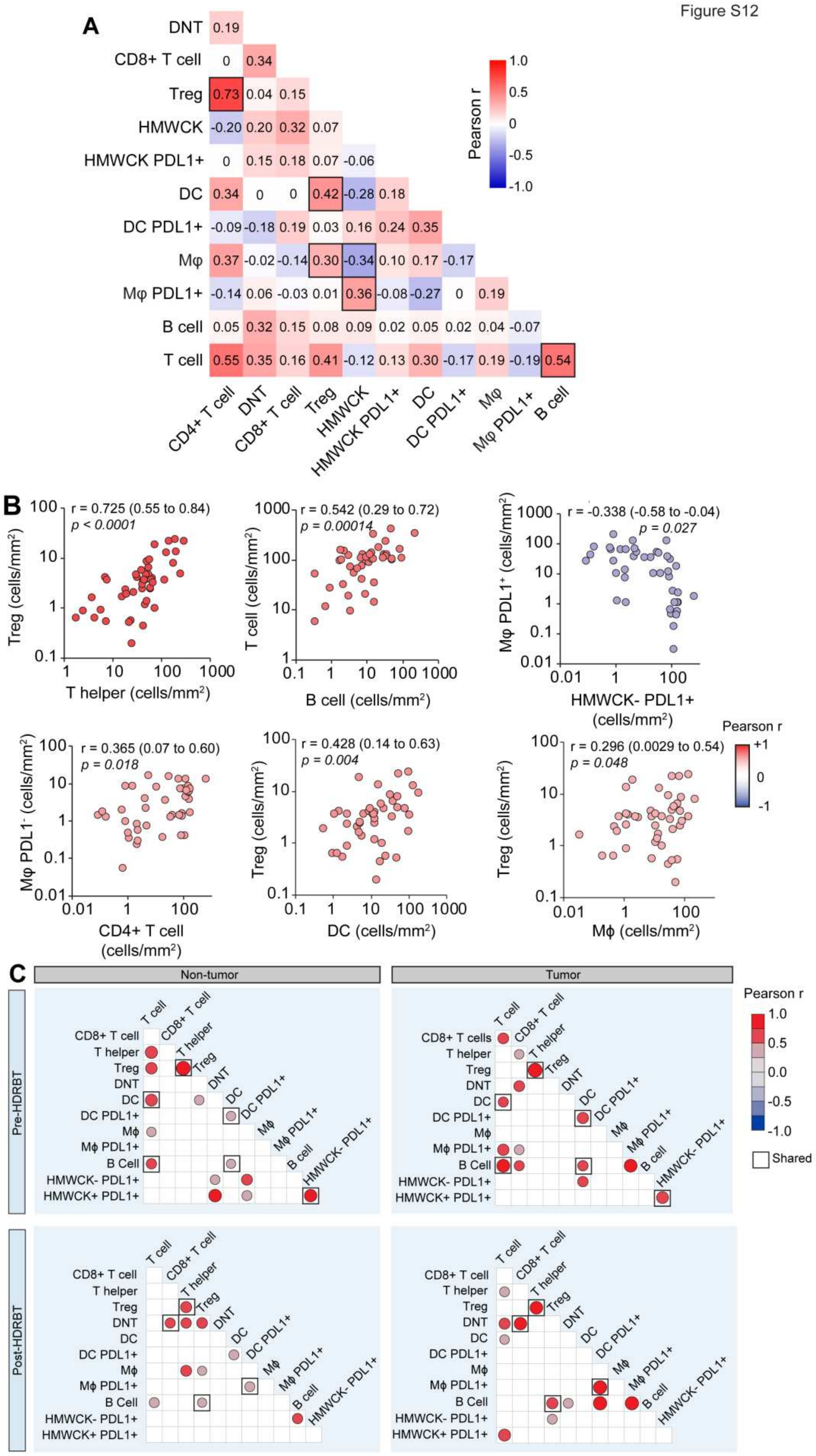

	CD4+ T cell	DNT	CD8+ T cell	Treg	HMWCK	HMWCK PDL1+	DC	DC PDL1+	Mφ	Mφ PDL1+	B cell
DNT	0.19										
CD8+ T cell	0	0.34									
Treg	0.73	0.04	0.15								
HMWCK	-0.20	0.20	0.32	0.07							
HMWCK PDL1+	0	0.15	0.18	0.07	-0.06						
DC	0.34	0	0	0.42	-0.28	0.18					
DC PDL1+	-0.09	-0.18	0.19	0.03	0.16	0.24	0.35				
Mφ	0.37	-0.02	-0.14	0.30	-0.34	0.10	0.17	-0.17			
Mφ PDL1+	-0.14	0.06	-0.03	0.01	0.36	-0.08	-0.27	0	0.19		
B cell	0.05	0.32	0.15	0.08	0.09	0.02	0.05	0.02	0.04	-0.07	
T cell	0.55	0.35	0.16	0.41	-0.12	0.13	0.30	-0.17	0.19	-0.19	0.54

Figure S13

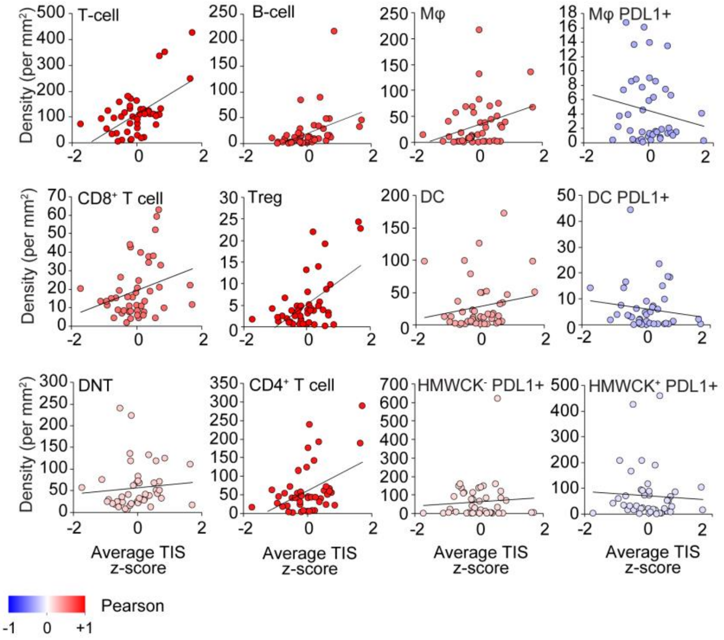
Density (per mm^2)
T-cell
B-cell
Mφ
Mφ PDL1+
CD8$^+$ T cell
Treg
DC
DC PDL1+
DNT
CD4$^+$ T cell
HMWCK$^-$ PDL1+
HMWCK$^+$ PDL1+
Average TIS z-score
Pearson
-1
0
+1

Figure S14

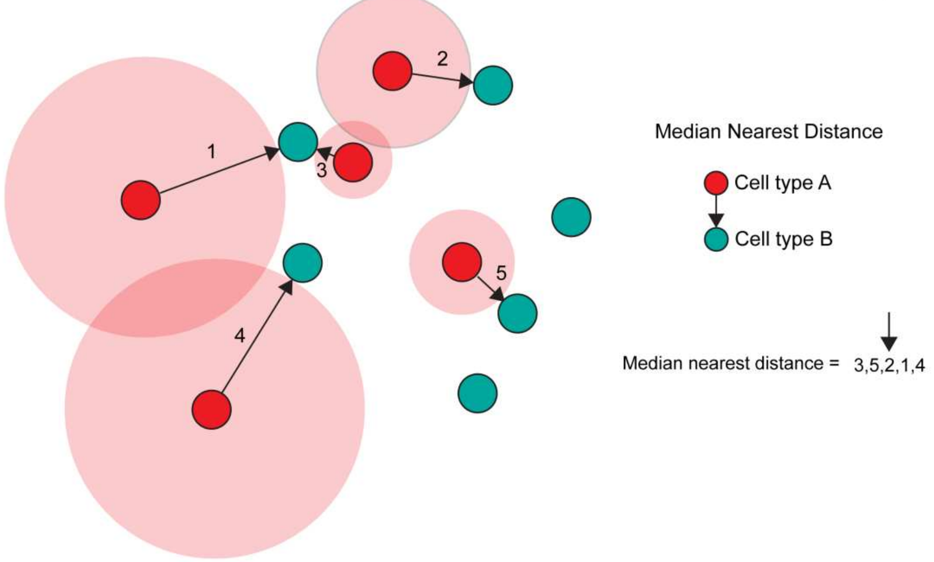
2
1
3
4
5
Median Nearest Distance
Cell type A
Cell type B
Median nearest distance = 3,5,2,1,4

Supplementary References

1. Halse, H., et al., *Multiplex immunohistochemistry accurately defines the immune context of metastatic melanoma.* Sci Rep, 2018. **8**(1): p. 11158.
2. Keam, S.P., et al., *The Transcriptional Landscape of Radiation-Treated Human Prostate Cancer: Analysis of a Prospective Tissue Cohort.* Int J Radiat Oncol Biol Phys, 2018. **100**(1): p. 188-198.
3. Keam, S.P., et al., *Biodosimetric transcriptional and proteomic changes are conserved in irradiated human tissue.* Radiat Environ Biophys, 2018. **57**(3): p. 241-249.
4. Tyanova, S., et al., *The Perseus computational platform for comprehensive analysis of (prote)omics data.* Nat Methods, 2016. **13**(9): p. 731-40.
5. Subramanian, A., et al., *Gene set enrichment analysis: a knowledge-based approach for interpreting genome-wide expression profiles.* Proc Natl Acad Sci U S A, 2005. **102**(43): p. 15545-50.
6. Danaher, P., et al., *Pan-cancer adaptive immune resistance as defined by the Tumor Inflammation Signature (TIS): results from The Cancer Genome Atlas (TCGA).* J Immunother Cancer, 2018. **6**(1): p. 63.